Review of Scientific Instruments

Low-profile self-sealing sample transfer flexure box

Cite as: Rev. Sci. Instrum. **88**, 083705 (2017); https://doi.org/10.1063/1.4997952
Submitted: 09 March 2017 • Accepted: 26 July 2017 • Published Online: 25 August 2017

Kevin Simon, Lukas Porz, Tushar Swamy, et al.

AIP Publishing

Low-profile self-sealing sample transfer flexure box

Kevin Simon,[1] Lukas Porz,[2,a)] Tushar Swamy,[1] Yet-Ming Chiang,[2] and Alexander Slocum[1,b)]
[1]*Department of Mechanical Engineering, Massachusetts Institute of Technology, Cambridge, Massachusetts 02139, USA*
[2]*Department of Materials Science and Engineering, Massachusetts Institute of Technology, Cambridge, Massachusetts 02139, USA*

(Received 9 March 2017; accepted 26 July 2017; published online 25 August 2017)

A flexural bearing mechanism has enabled the development of a self-sealing box for protecting air sensitive samples during transfer between glove boxes, micro-machining equipment, and microscopy equipment. The simplicity and self-actuating feature of this design makes it applicable to many devices that operate under vacuum conditions. The models used to design the flexural mechanism are presented in detail. The device has been tested in a Zeiss Merlin GEMINI II scanning electron microscope with Li_3PS_4 samples, showing effective isolation from air and corrosion prevention. *Published by AIP Publishing.* [http://dx.doi.org/10.1063/1.4997952]

I. INTRODUCTION

Transferring air sensitive samples between scientific imaging equipment is challenging because standard Scanning Electron Microscopes (SEMs) and other processing equipment often lack airtight transfer systems. Improper handling of air-sensitive samples can allow extensive chemical reaction. Exposure to oxygen, water vapor, or other contaminants must thus be prevented for research and quality control analyses.

Although other solutions exist for transferring air-sensitive samples, prior to this project, no low profile, self-actuating system has been produced. Howe *et al.* has developed a sample transfer system with a swinging lid, but it does not re-seal to preserve the samples after imaging.[1] Hall *et al.* developed a re-sealing system that couples with the rotation stage on a Philips 501 SEM, but it is not standardized for use with other instruments.[2] These devices, among the other sample transfer systems,[3–7] are limited in their use by the range of motion of the lid, inter-microscope compatibility, re-sealability, availability, and price.

Figures 1 and 2 show the Sample Transfer Flexure Box (STFB), designed and demonstrated in this work, which uses an arrangement of four-bar linkage flexures and an opposing piston, operated by the change in pressure in the SEM, to passively open and reseal the sample chamber with minimal vertical motion. The resulting system is effective, low cost, and compatible with many SEMs and other advanced microscopy and micro-machining equipment such as focused ion beam (FIB) instruments.

II. FUNCTIONAL REQUIREMENTS AND DESIGN PARAMETERS

The design process began with the definition of the critical functional requirements that satisfy the needs of the end user. The functional requirements were determined through unstructured interviews and observation of different experimental procedures. Once the functional requirements were specified, they were translated into measurable design parameters, which drive the design and analysis of the STFB. Both the functional requirements and the design parameters are presented in Table I.

Functional requirements 1 and 6 arise because sensors, ion guns, or other sensitive equipment are often within 10 mm of the focal plane. In a FIB, the sample stage is rotated about 2 orthogonal axes, meaning that a loose lid can crash into the instruments. Protecting the instrument in which the STFB is used is essential to the utility of this device.

Functional requirement 3 also motivates the use of linear flexural elements. Rotating lids apply uneven forces on the seal because different parts of the seal are at different lever-arm lengths. Linear flexures are natural countermeasures to this risk. A linear motion device can more evenly apply force to the seal. Functional requirements 2, 4, and 5 are all necessary for the device to be of use for imaging air-sensitive samples.

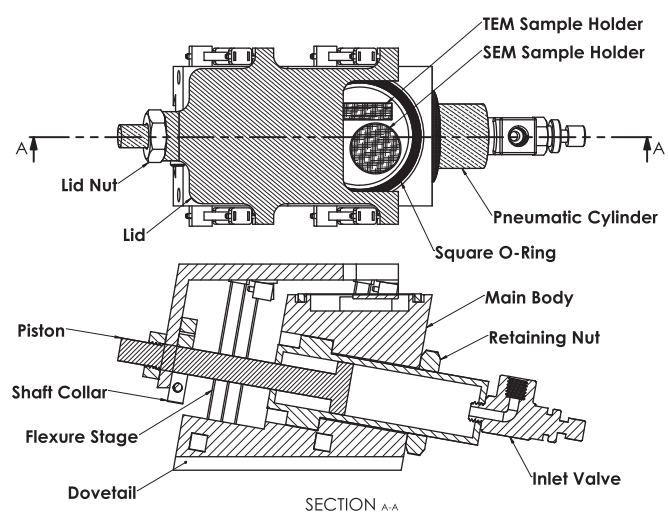

FIG. 1. A top and cross section schematic of the Sample Transfer Flexure Box (STFB) in an open state.

[a)]Current address: Institute of Materials Science, Technische Universität Darmstad, Darmstadt 64287, Germany.
[b)]Electronic mail: Slocum@mit.edu

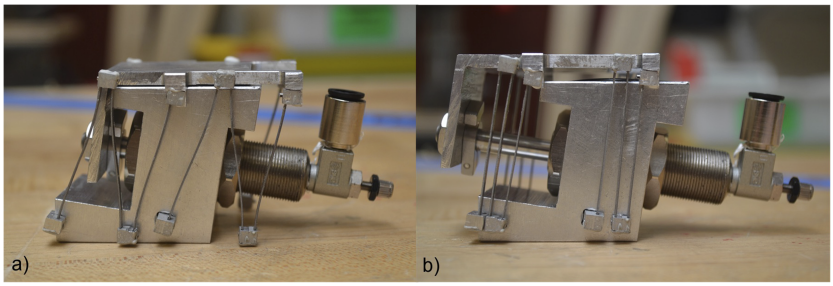

FIG. 2. The STFB in closed (a) and open (b) state on a workbench, with vacuum applied to the cylinder to simulate operation in a vacuum environment.

TABLE I. The functional requirements and design parameters necessary to achieve the desired performance.

No.	Functional requirement	Design parameter
1	Open in small headspace	Lid vertical travel <5 mm
2	Expose a SEM pin and TEM grid	Lid horizontal travel >15 mm
3	Maintain air-tight seal	Evenly compress seal by 1%–5% of the seal height
4	Open for imaging	Open in response to a medium ambient vacuum
5	Close after work	Trigger at 1 atm ambient
6	Fit in SEM + FIB	Modular bottom; maximum height <50 mm; maximum length <100 mm; maximum width <75 mm
7	Not damage equipment	Predictable, fail safe, no sliding, no ferromagnetic materials
8	Work repeatably	Low off-axis loading

Functional requirement 7 requires that the lid, flexures, and piston have no ferromagnetic elements because some instruments induce a large magnetic field. Sliding elements must also be avoided if the STFB is to be used frequently. Sliding elements wear after regular use, particularly in a vacuum environment where lubrication is limited. Wear can leave fine particles inside in the machine or on the sample. In discussions with users, some FIB operators have said that any risk of producing wear particles is unacceptable.

Repeatability is necessary to ensure consistent sealing. Because load-induced geometric errors are small, friction is the biggest challenge to repeatability. Functional requirement 8 requires the minimization of off-axis loading on the piston to minimize the risk of the piston sticking. Assuming that the coefficient of friction in a vacuum environment is approximately 1, the off-axis force must be less than $1/20^{\text{th}}$ the piston force to make friction forces negligible compared to the piston force. Assuming that the leverage on the piston is approximately 10, the acceptable parasitic moment must be less than $1/200^{\text{th}}$ the piston force to keep moment-induced friction similarly negligible.

III. DESIGN AND CONSTRUCTION

The selected design, which meets all of the functional requirements and design parameters, is a double-acting piston opposed by an array of 4 parallel 3-stage blade flexures. The double acting piston has one port exposed to ambient pressure. The other port is sealed and held below −84 kPa gauge pressure. In this configuration, the lid is held closed by the piston under atmospheric ambient pressure and is opened by the flexures in ambient vacuum. When work with the STFB in an open, vacuum state is finished, the work chamber is filled with an inert gas. The ambient pressure then closes the STFB, protecting the sample with inert gas. Because the flexures are in a relaxed state when the STFB is open in ambient vacuum, this design ensures that structural failures on the box will not damage the instrument.

To combine the horizontal and vertical motion, the piston and flexure stages are rotated 10° from the rest of the STFB. This angle of motion, shown in Fig. 5, provides 3.6 mm of vertical and 20.4 mm of horizontal travel. When open, the lid is below the instrumentation and gives a wide work area.

The embodiment of the design principles presented is composed of an aluminum body with titanium flexures. The body of the STFB is CNC milled out of aluminum for stability in a vacuum environment and because it is easily machined for prototyping. The flexures are made of titanium strips, cut on a water jet. Titanium was selected for its ratio of stiffness to yield stress, which minimizes the flexure length required to achieve the target lid deflection. The flexures are connected by aluminum mounting blocks with 2 press-fit 1 mm stainless steel spring-pins at each attachment point to constrain the blades. Each flexure stage mates with the body in machined slots and is clamped in place by setscrews. Torr Seal™, a vacuum-grade epoxy, attaches the flexures to the lid at a mounting block with a mating feature.

The top of the STFB has a pocket with features that can hold a SEM sample-holding pin and a transmission electron microscope (TEM) grid. This allows for transfer of the sample directly to a SEM or to a sealed TEM sample holder, via a glovebox, after work in a FIB. Around this pocket is a square O-ring. Square O-rings resist twisting forces induced by the lid as it makes contact with a tangential motion component and provide a longer leak-path at low compression. The bottom of the lid is lapped to a mirror finish to ensure a good seal.

IV. DETAILED DESIGN

The design of the STFB is driven by the force associated with vacuum pressure. The selected commercially available piston has a 12.4 mm diameter bore. Neglecting friction, this

piston nominally provides 12.5 N of force with 1 atm pressure across the piston. Providing a margin for manufacturing errors, friction on the piston seal, and additional force for the seal, the return flexures are sized to provide approximately 8 N of reaction force when fully extended at 20.2 mm.

Preliminary flexure design uses a linear bending beam model and is refined with a large-deflection finite difference model. The simplest topology for a 1 degree of freedom flexure is 2 or more parallel blade flexures.[8] Flexure geometry and the number of stages determine the lid's stiffness and range of motion through Eqs. (1)–(4),

$$F = k_f x, \tag{1}$$

$$k_f = \frac{12EI}{pl^3}, \tag{2}$$

$$M = \frac{Fl}{2}, \tag{3}$$

$$\sigma_b = \frac{Mt}{2I} = \frac{Flt}{4I} = \frac{3Ext}{pl^2}. \tag{4}$$

F is the force at the tip of the flexure; k_f is the stiffness of a blade flexure with parallel motion; E is Young's modulus; I is the second moment of inertia; x is the tangential displacement of the tip; L is the length of the flexure; p is the number of parallel flexure stages; σ_b is the maximum flexural bending stress; t is the thickness of the flexure blade. Given the 50 mm limit on height, 10° angled flexure motion over 20 mm, and 8 mm of height for mounting the flexures, a nominal flexure length of 38 mm fits within the constraints. With 0.406 mm thick, 2 mm wide grade 5 titanium (E = 114 GPa, σ_{yield} = 830 MPa) flexure blades, Eq. (4) predicts that three stage flexures, depicted in Fig. 3, will stay below their yield stress over a range of motion of 20.2 mm. This topology results in a maximum stress of 742 MPa, which gives an acceptable factor of safety of 1.1. The expected factor of safety predicted by the detailed, nonlinear model will be greater because higher-order beam models predict lower stiffness. Two flexures are unable to provide the range of motion in the space without yielding. Four flexures would also accomplish the same goal but do not provide increased functionality. With the basic flexure topology selected, a non-linear finite difference model is used to refine the flexure model and minimize parasitic forces.

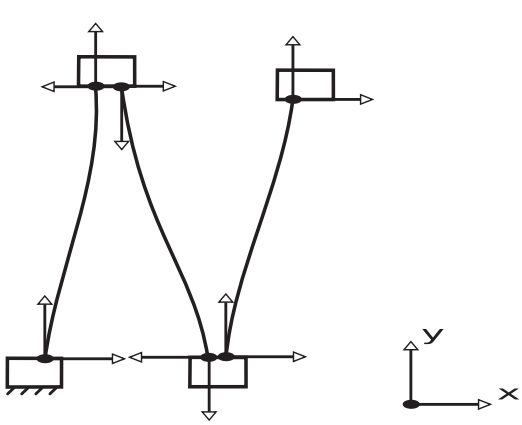

FIG. 3. The topology of one of the parallel flexure stages. The different coordinate systems on the structure represent the location and rotation of different homogenous transformation matrices.

The finite difference model assumes that tip forces translate and rotate with the tip of the flexure. Beginning with an applied moment and force at the tip, the finite difference model steps backwards along the length of the flexure with Eq. (5), computing new moments via Eq. (6) and incrementally rotating the trailing edge of the beam by Eqs. (7) and (8) until the length of the beam has been traversed. This scheme is depicted in Fig. 4,

$$r_i = r_{i-1} - N_i ds, \tag{5}$$

$$M_i = M_{i-1} - r_i \times F, \tag{6}$$

$$d\theta_i = \frac{-M_i ds}{EI}, \tag{7}$$

$$N_{i+1} = \begin{bmatrix} 1 & -d\theta_i \\ d\theta_i & 1 \end{bmatrix} N_i. \tag{8}$$

Here, r_i is the vector from the tip of the beam to the ith segment; N_i is the normal vector of the ith section; M_i is the internal moment generated at the ith section; ds is the segment length; and $d\theta_i$ is the rotation angle of the segment normal vector over the length of the ith segment. Once the rotation of each beam element is computed, Eq. (9) describes the rotation of each beam segment relative to the base rotation, producing a new set of normals, G_i, in the ground coordinate system. R_n is the rotation matrix of the nth segment, the ground, in the tip's coordinate system. Equation (10) integrates the segment normals to calculate D, the displacement of the tip in the ground coordinate system,

$$G_i = R_n N_i, \tag{9}$$

$$D = \sum G_i ds. \tag{10}$$

This method ensures that the base of the beam has the correct orientation. The final tip position and rotation are turned into a homogeneous transformation matrix. That homogeneous transformation matrix can be used to predict the primary motion and also predict parasitic deflections from manufacturing tolerances that may prevent the lid from properly sealing.[9] Homogeneous transformation matrices of the flexure deflection and rigid flexure connections model the propagation of forces and moments through the system. Figure 5 shows how homogenous transformations, H, can translate the moments and forces between the different reference frames shown in Fig. 3. The finite difference flexure model shows that a three-stage flexure with a 38 mm ground stage, 38 mm mid stage, and 35 mm end stage, as shown in Fig. 6, enables a compact

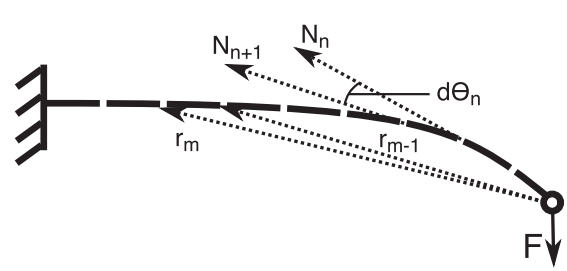

FIG. 4. A graphic representation of the finite difference scheme. The indices "m" and "n" represent two different elements instead of "i" in Eqs. (5)–(8). The different subscripts, depicted at two different locations, were chosen for consistency and clarity.

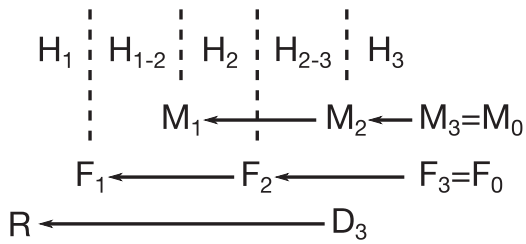

FIG. 5. Diagram of the propagation of moments, forces, and displacements through the flexure system.

design with sufficiently small parasitic loading,

$$M_k = M_{k+1} - \left(\prod_{j=3}^{k+1} H_j\right) F_0 \times D_{k+1}, \tag{11}$$

$$F_k = \left(\prod_{j=3}^{k-(k+1)} H_j\right) F_0, \tag{12}$$

$$H_k = f\left(F_k, M_k\right), \tag{13}$$

$$R = \left(\prod_{j=2-3}^{1} H_j\right) D_3, \tag{14}$$

where R is the displacement of the flexure end in the ground reference frame; D_k is the tip displacement of the kth flexure; $f(F_k, M_k)$ is the function which computes displacement and rotation of the kth flexure stage as described above. This framework is a common method for describing the error and motion of precision machines. It can be extended to different flexure topologies. Since flexure tip rotation and displacement can be efficiently computed from moments and forces, the inverse problem is solved with a nonlinear root-finder. The solution to this inverse problem yields the forces and moments that the linear translation of the piston induces,

$$P_x = -4F_x, \tag{15}$$

$$P_y = -4F_y, \tag{16}$$

$$M_p = 2F_x(y_1 + 2y_2) - 2F_y(x_1 + 2x_2) - M_f. \tag{17}$$

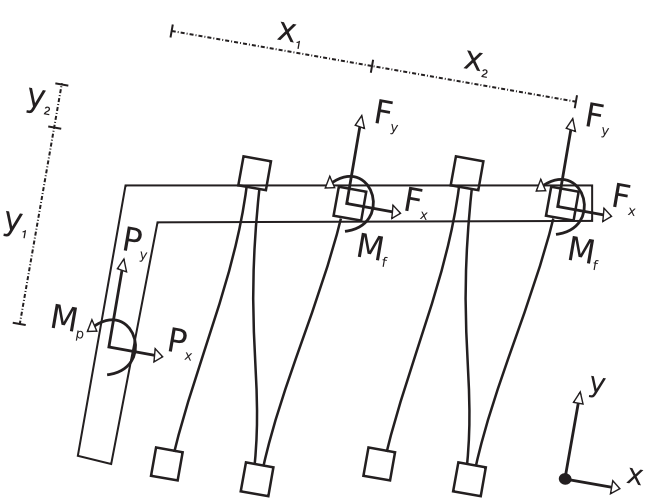

FIG. 6. The layout and loading of the STFB lid.

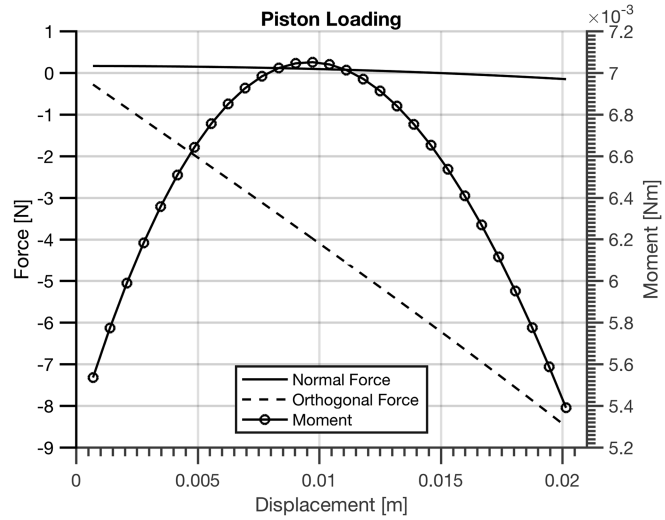

FIG. 7. The loading of the piston across the optimal lid's range of motion.

Equations (15)–(17) are based on the free-body diagram in Fig. 6. These equations provide the expected loading of the piston as it travels through the lid's range of motion. F_x and F_y are the x and y components of the flexure force vector, computed in Eq. (12). M_f is the moment about the Z axis applied by the flexure, computed in Eq. (11). The factor of 4 in the equations emerges because there are four flexure stages, each one applying F_x and F_y to the lid. A design where x_1 = 30 mm, x_2 = 17.1 mm, y_1 = 5.3 mm, and y_2 = 14.7 mm fits the range of motion, compactness, and parasitic loading functional requirements. In this case, a solution to this inverse problem was found with a nonlinear solver. The model predicts a maximum stress of 455 MPa with this design, giving a final factor of safety of 1.8.

Figure 7 shows that the off-axis loading and parasitic moment induced by a linear translation of 20.2 mm are within the specifications of functional requirement 8. There are other topologies that can further reduce the parasitic loading. For example, a serial 4-stage blade flexure will nearly eliminate the off-axis parasitic force but increase complexity and reduce off-axis stiffness.

V. SYSTEM PERFORMANCE

The scientific instruments to which the STFB can be applied depend primarily on the quality of the seal. Better sealing enables applications with more air sensitive materials. To test the effectiveness of the design, we performed SEM examinations with and without the STFB of Li_3PS_4, a highly air-sensitive material that is the basis for solid electrolyte membranes proposed for use in all-solid-state batteries.[10] Upon exposure to air, the material develops a pattern of surface cracks within seconds. These cracks are a visible indicator of degradation from atmospheric exposure, as shown in Fig. 8(a). It is imperative for battery development or production quality control that samples of such atmospheric sensitivity can be transferred from a protected environment, such as a glovebox,

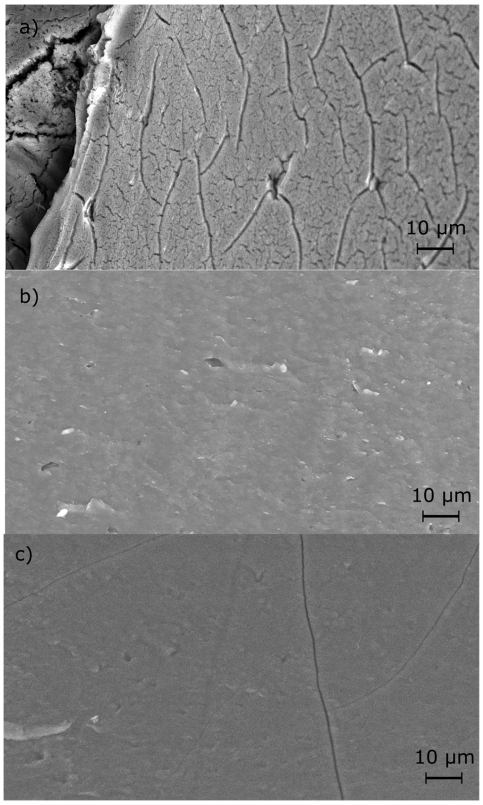

FIG. 8. An electron micrograph of Li_3PS_4 sample after direct exposure to air (a), after 10 min transport with the STFB (b), and after 10 h in the STFB (c).

to a SEM for examination. Whether the surface cracks shown in Fig. 8(a) form is a useful metric for the level of protection.

In a scanning electron microscope, in this case the Zeiss Merlin GEMINI II, it takes 20 s to transfer a sample from a sealed carrier into the microscope via the airlock. Unprotected, this exposure results in intense mud-crack patterns in the sample, making analysis impractical. While using the STFB to transfer a Li_3PS_4 sample from the glovebox to the SEM in a comfortable time span of 10 min (including the pumping time of the main chamber), surface cracks were absent, as shown in Fig. 8(b). Since aluminum absorbs some moisture and oxygen, the inside of the STFB was degassed in a vacuum chamber for 10 h before testing.

To fully characterize the prototype, the leakage rate has to be tested over a longer period of time. Letting the closed STFB sit in air for 10 h before inserting it into the SEM results in few individual cracks in the sample, as shown in Fig. 8(c). However, there is no practical reason why a sample cannot be transferred in less than an hour. Hence, these tests demonstrate sufficient functionality of the STFB for use with air sensitive samples similar to Li_3PS_4.

VI. CONCLUSION AND FUTURE WORK

The design and performance of a device for preserving air sensitive materials during transfer between a glovebox and instrumentation have been presented. The functional requirements, design principles, and analytical equations have been presented in detail. The functionality of the STFB has been demonstrated with Li_3PS_4 samples in a Zeiss Merlin Gemini II SEM.

The design analysis and testing show that repeatable motion with minimal parasitic loading is possible with 3 serial flexures. Further reductions in parasitic loading and device size can be achieved with 4 serial flexures but increased complexity. Friction in the piston is still a possible source of non-repeatability. Replacing the piston with a welded metal bellows would eliminate friction in the mechanism.

The STFB for air sensitive samples is valuable to research that use SEMs, FIB instruments, or other vacuum based instruments for studying battery materials, semiconductor processing, nano-materials, or similar research topics. Although several designs have been produced before, none of them combine all of the features necessary for low-profile safe, frequent, and reliable use presented here.

ACKNOWLEDGMENTS

This work made use of the MRSEC Shared Experimental Facilities at MIT supported by the National Science Foundation under Award No. DMR-1419807. We thank Patrick Boisvert for assistance and training in SEM operation. The authors gratefully acknowledge support from the U.S. Department of Energy's Office of Basic Energy Science for the Chemomechanics of Far-From-Equilibrium Interfaces (COFFEI) small group, through Award No. DE-SC0002633 (J. Vetrano, Program Manager). The authors also wish to thank the Tata Center at MIT for supporting Kevin Simon's research assistantship.

[1]J. Y. Howe, L. A. Boatner, J. A. Kolopus, L. R. Walker, C. Liang, N. J. Dudney, and C. R. Schaich, J. Mater. Sci. **47**, 1572 (2012).
[2]J. B. Hall and P. P. Hruskoci, Scanning **4**, 175 (1981).
[3]C. Solliard and M. Rappaz, Rev. Sci. Instrum. **49**, 101 (1978).
[4]R. M. Gaume and L.-M. Joubert, Rev. Sci. Instrum. **82**, 123705 (2011).
[5]L. W. Hobbs, J. Phys. E: Sci. Instrum. **3**, 85 (1970).
[6]B. Gamer and R. Monig, "Atmospheric-sensitive sample e.g. lithium material, transporting device for use in scanning electron microscope, has component with positioning device e.g. sample holder, for two spatial axes and rotation axis and grip device for cover," DE patent 102,008,062,080 (2010).
[7]P. Marek and T. Scherer, "Self-opening vacuum can/box," WO patent 2013/178,218 (2013).
[8]J. Hopkins, "Design of parallel flexure systems via freedom and constraint topologies (FACT)," M.S. thesis, Massachusetts Institute of Technology, 2007.
[9]A. Slocum, *Precision Machine Design*, 1st ed. (Society of Manufacturing Engineers, Dearborn, Michigan, 1992).
[10]Z. Liu, W. Fu, E. A. Payzant, X. Yu, Z. Wu, N. J. Dudney, J. Kiggans, K. Hong, A. J. Rondinone, and C. Liang, J. Am. Chem. Soc. **135**, 975 (2013).